Research Square

Preprints are preliminary reports that have not undergone peer review.
They should not be considered conclusive, used to inform clinical practice,
or referenced by the media as validated information.

Structural evolution and combustion energy of Al-B clusters

Elizaveta E. Vaneeva

Elizaveta.Vaneeva@skoltech.ru

Skolkovo Institute of Science and Technology

Anastasiia A. Mikhailova

Skolkovo Institute of Science and Technology

Sergey V. Lepeshkin

Skolkovo Institute of Science and Technology

Alexey P. Maltsev

Skolkovo Institute of Science and Technology

Artem R. Oganov

Skolkovo Institute of Science and Technology

Research Article

Keywords:

Posted Date: May 18th, 2026

DOI: https://doi.org/10.21203/rs.3.rs-9334205/v1

License: This work is licensed under a Creative Commons Attribution 4.0 International License.
Read Full License

Additional Declarations: No competing interests reported.

Abstract

Systematic structure prediction of Al_nB_m clusters ($0 \le n, m \le 16$) was performed to explore their structural diversity, stability, and combustion-related properties. We identified structural motifs that evolve with boron content, ranging from isolated boron atoms embedded in aluminum frameworks to dense and perforated boron networks.We have analyzed the stability of Al_nB_m molecules using criteria adopted in nanocluster studies, where relative stability with respect to neighboring compositions serves as an indicator of “magic” clusters. Fragmentation analysis indicates that mixed Al_nB_m clusters typically dissociate through the loss of a single aluminum atom. At the nanoscale, pure boron and boron-rich Al_nB_m clusters exhibit higher Gibbs free energies of combustion than aluminum clusters, in contrast to bulk behavior. Specific combustion energies for boron nanoclusters are higher too. Smaller clusters exhibit larger energy output because of their higher fraction of reactive surface atoms, although this size-dependent effect becomes less pronounced upon aluminum incorporation.

1. Introduction

The development of high-energy-density fuels is a key challenge for next-generation propulsion and power systems. One promising approach is the incorporation of metal or metalloid nanoclusters into conventional liquid hydrocarbon fuels.[1] Due to their small size, nanoclusters possess a large fraction of surface atoms, which makes them highly reactive and allows for faster and more complete oxidation during combustion. This often results in increased heat release, shorter ignition delay, and faster flame propagation.[2] Among the various candidates, particularly aluminum and boron are the most widely explored. Their relatively low ignition temperatures, high heats of combustion, and compatibility with liquid-fuel formulations make them especially effective in improving the performance of traditional hydrocarbon fuels.[3] Both elements belong to group 13 and are isoelectronic, having three valence electrons, yet they exhibit different bonding characteristics and physical behavior. Aluminum has relatively diffuse valence orbitals, which give rise to delocalized, weakly directional metallic bonding, hence, it has a relatively low surface energy: breaking metallic bonds and forming surfaces is energetically inexpensive, and dangling bonds are not strongly penalized. Boron, in contrast, forms strongly directional, 2-center and multicenter covalent bonds and behaves as a frustrated semiconductor. In such systems, dangling bonds are energetically costly, leading to high surface energies and pronounced surface reconstruction.

These electronic differences that govern the structural chemistry of aluminum and boron are directly reflected in their preferred cluster geometries. Small aluminum clusters favor compact, highly symmetric structures, most notably the icosahedral Al_{13} “magic” cluster, and icosahedral motifs are also common in aluminum-based quasicrystals. In contrast, crystalline boron consists of hollow B_{12} icosahedra arranged in complex networks, yet such units are absent in small free boron clusters, which instead adopt planar or quasi-planar structures over a wide size range. [28] Another important distinction lies in

bond strengths. A single B–B bond (3.08 eV)[7] is significantly stronger than a single Al–Al bond (1.37 eV)[7] due to its covalent nature.

From an energetic perspective, boron has long been considered as one of the most promising energetic additives for hydrocarbon fuels due to its exceptionally high gravimetric (≈ 58 MJ/kg) and volumetric (≈ 131 MJ/L) energy densities.[3] Its combustion releases large amounts of heat and can significantly increase the flame temperature, thereby improving the thermal efficiency and thrust of propulsion systems. However, the practical utilization of boron remains challenging. Although boron has a higher energy density than aluminum, its practical use is hindered by the rapid formation of a dense, B_2O_3 layer that blocks oxygen diffusion to the boron core, leading to incomplete combustion and the generation of solid oxide particles that ultimately reduce performance and can cause nozzle clogging.[4][5] As a result, boron exhibits long ignition delays, incomplete oxidation, and reduced overall energy release.[6] These limitations hinder its direct use in propulsion systems despite its outstanding theoretical energy content.

Aluminum, in contrast, ignites at lower temperature and exhibits faster oxidation kinetics under combustion conditions than boron, which together with its high heat of combustion (~ 31 MJ/kg) makes it an effective additive and ignition promoter in propellants and explosives.[7] When aluminum and boron are combined, the rapid ignition of aluminum can slow down the growth of the B_2O_3 layer and partially disrupt the existing oxide film. As a result, oxygen gains easier access to the boron, enabling more complete oxidation and, consequently, more complete boron combustion.[5] Such mixed clusters or composite additives retain high theoretical energy density of boron while benefiting from superior ignition and oxidation characteristics of aluminum, making Al–B materials attractive candidates for next-generation high-energy fuels.

However, clusters of mixed compositions (Al_nB_m) have not been investigated properly until now. The experimental study of these clusters is a difficult task, therefore, it is advisable to start by identifying the most promising of them at the fundamental level. Only a few studies addressed the analysis of structure and properties of certain neutral Al_nB_m clusters of special composition: Al_nB_m ($n + m \leq 7$) [8] and AlB_n ($n = 0 - 20$).[9][10] Thus, most existing studies are limited to examining only a small number of fixed compositions, whereas multicomponent clusters, which are of greater interest for practical applications, may have unexpected stoichiometries not found at the macro scale.

In this work, we conducted a systematic study of Al_nB_m nanoclusters in a wide compositional range ($0 \leq n \leq 16$, $0 \leq m \leq 16$). We utilize global optimization methods in conjunction with density functional theory (DFT) calculations to determine ground-state structures. We also investigate the reactive (energetic) characteristics of Al–B clusters, including combustion energy that indicates their potential energy release upon oxidation, and identify the most stable (“magic”) compositions to elucidate the structure–stability relationships.

2. Computational Methods

The structures of Al_nB_m clusters were determined using an evolutionary variable-composition global optimization algorithm implemented in the USPEX code. [9, 10]. To ensure accurate and reliable structure prediction, the computational procedure consisted of several steps. First, the USPEX search was performed using an evolutionary algorithm in combination with the ab initio VASP code [11],[12], which employs the projector-augmented wave method[13] and the Perdew–Burke–Ernzerhof (PBE) exchange-correlation functional.[14] Spin polarization was taken into account during these calculations. Subsequently, the 10 lowest-energy isomers from each composition were selected for further refinement using the GAUSSIAN software,[15] applying the B3LYP hybrid functional [16, 17] and the 6-311G+(d,p) basis set, using spin multiplicity corresponding to the lower energetic state.[18] We calculated the vibrational frequencies in all obtained structures and verified that each possesses 3N-6 positive frequencies. For each ground state structure we calculated Gibbs free energy at T = 300K, applying partition functions both for vibrations, translations, rotations, and electronic configurations. The structural stability was assessed using the local stability, $\Delta^2_{min}(n, m)$, and fragmentation energy (E_{frag}) as described in our previous studies.[19–26]

3. Results and Discussion

3.1. Structure and stability of nanoclusters

We explored the ground-state structures of Al_nB_m clusters within a broad compositional range of $0 \le n, m \le 16$. The *xyz* coordinates of all optimized ground-state structures are provided in ESI Section S2.

Our results reproduced previous calculations for smaller clusters AlB_m (m = 0–20) [9, 10], Al_nB_m ($n + m \le 7$).[8, 27]. The ground-state structures of Al_nB_m (up to $0 \le n, m \le 16$) clusters were found for the first time. The ground-state structures of Al_nB_m nanoclusters can be classified into several distinct classes based on the structural characteristics of the boron fragments within each cluster (Fig. 1). Al-rich Al_nB_m nanoclusters ($m \le 4$ and $n + m \ge 7$) form *1st class* (Fig. 1a). The clusters have a non-planar structure: an aluminum framework with a small isolated boron fragment inside. As the boron content increases, boron replaces aluminum, starting from the inner sites and moving outward, while the atomic arrangement remains fixed.

The *second class* of Al_nB_m (Fig. 1b) nanoclusters is defined by dense boron fragments that form well-organized nets. Unlike Al-rich clusters, the boron atoms interact closely, forming continuous or semi-continuous networks that resemble fragments of larger boron sheets. Depending on the aluminum environment, nets could be planar, quasi-planar (exhibit a nearly planar geometry with slight deviations). There are the exceptions with non-planar boron motifs with $5 \le m \le 7$. Notably, these boron networks correspond to the ground states of pure boron clusters.[28] Planar and quasi-planar nets are forming hexagonal or distorted hexagonal patterns, akin to borophene-like structures.[29] Structures along the diagonal $n + m$=22 exhibit pronounced layered motifs, reminiscent of those found in bulk aluminum

boride AlB_2. However, unlike the planar boron layers observed in the bulk phases, the boron-rich fragments in these clusters adopt curved, nonplanar geometries.

As the boron concentration increases, aluminum atoms become embedded within the dense boron networks, displacing boron fragments and causing deviations from ideal compact structures (dense networks). Here gaps and irregularities appear, as if the once-unbroken sheet has been stretched and torn apart in places. This leads to the formation of a distinct class (*class 3*, Fig. 1c) of Al_nB_m clusters known as perforated networks. It is worth noting that chain-like structures formed by boron in structures with $n + m \geq 24$ are generally energetically unfavorable — previous studies consistently show boron's tendency to form tubular, cage-like and core-shell configurations. These perforated networks can be considered as transition states from dense nets to tubular or cage-like boron structures, such as B_{19} (D_{2d}) or the highly symmetric B_{20} (D_{10d}).[28] However, in this case, the incorporation of aluminum appears to stabilize such unconventional boron fragments by providing a metallic framework that supports the existence of perforated networks. Such structural modifications significantly impact the local stability of the clusters.

Most of the small Al_nB_m clusters ($n + m \leq 6$ and $m \leq 4$) are categorized as *class 4* (Fig. 1d) adopt a planar arrangement, with the exception of Al_2B_2 and Al_3B_4, where boron atoms are repelled by aluminum, leading to a distorted geometry.

The stability of binary nanoclusters, characterized by Δ^2_{min} and E_{frag}, can be effectively visualized using 2D heatmaps (Fig. 2). In Fig. 2a, red regions indicate highly stable magic clusters, while blue areas represent unstable compositions where $\Delta^2_{min} < 0$. Light blue regions correspond to unstable molecules, where $-0.4\ eV \leq \Delta^2_{min} \leq 0$.

An initial examination of the stability maps reveals distinct diagonal stability trends at $n + m$ = 6, 12, 16, 18, 20, and 22, particularly visible in the Δ^2_{min} map. Clusters along these diagonals exhibit closed-shell electronic structures and are predominantly associated with dense boron nets. For instance, clusters on the $n + m$ = 6 diagonal transition from pure 3D-shaped Al_6 to planar B_6, where boron atoms gradually replace aluminum, ultimately forming a separate boron sheet. Analogously, along the $n + m$ = 12, 16, and 18 diagonals, clusters evolve from pure aluminum to Al-rich compositions, then to structures with dense boron nets, and finally to pure boron clusters. In contrast, clusters along the $n + m$ = 20 and 22 diagonals are mainly composed of dense boron nets, which progressively transition into perforated boron structures. The upper right triangle of the Δ^2_{min} map (where $n + m \geq 24$), which primarily includes Al_nB_m clusters with perforated boron nets, displays a negative Δ^2_{min} value. This is due to the chain-like arrangement of boron in these structures, a configuration not typically associated with stable boron frameworks. However, when the aluminum content decreases to four or five atoms, some perforated nets transition to a planar geometry, thereby gaining local stability. Notably, several clusters exhibit “magic” stability despite having an odd number of electrons, which is often associated with high

structural symmetry, as in B_3 (D_{3h}), B_5 (C_{2v}), AlB_8 (C_{7v}), Al_2B_7 (D_{7h}), Al_3 (D_{3h}), $Al_{12}B$ (D_{5d}), Al_{13} (I_h) and $Al_{14}B_9$ (C_2). However, magic behavior is not exclusively symmetry-driven, since several clusters without symmetry also display enhanced stability, including Al_3B_{14} (C_1), $Al_{12}B_{11}$ (C_1), $Al_{13}B_{10}$ (C_1), and $Al_{13}B_{12}$ (C_1).

The maps clearly highlight the magic Al_{13} cluster, which adopts an I_h geometry with one aluminum atom enclosed inside. This structure has been confirmed experimentally through mass-spectrometric, which demonstrated the enhanced stability and characteristic electronic configuration of the 13-atom aluminum icosahedron.[30] This structural arrangement contributes to its exceptional stability, as confirmed by the fragmentation map (Fig. 2b). Analysis of fragmentation behavior further demonstrates that these clusters are highly resistant to decomposition, with clusters most favorably losing a single aluminum atom with exception of pure boron clusters that tend to lose a boron atom instead, which is reflected in high values of fragmentation (Table S1, Section 1 of ESI).

We have used a third criterion, the HOMO–LUMO gap. (Fig. 2c) shows interpolated heatmaps of gaps for Al_nB_m nanoclusters. This gap is a key factor in determining the electronic properties of a cluster, such as its electronic polarisability (and, hence, reactivity). Nanoclusters with a wide HOMO-LUMO gap are typically less reactive and thus more easily survive interactions with other molecules. The largest HOMO–LUMO gaps are observed for the B_8 and AlB_8 clusters. This enhanced gap can be attributed to their high structural symmetry, which promotes electronic shell closure and reduces the density of electronic states near the Fermi level.

3.2. Prospects of Al-B nanoparticles in application of high energy density materials

We investigated the potential of Al_nB_m clusters as high-energy-density additives to organic fuels. We examined the combustion of any cluster into the most stable oxides of aluminum and boron. To better approximate real conditions, we consider the process at 300 K and ambient pressure, using Gibbs free energy.

We calculated the energy output obtained from burning a given cluster in an oxygen atmosphere, leading to the formation of stable products — Al_2O_3 and B_2O_3. We assume that each cluster reacts with O_2, producing Al_2O_3 and B_2O_3 with the corresponding stoichiometric coefficients:

$$Al_nB_m + ¾\,(n + m)O_2 \rightarrow ½nAl_2O_3 + ½mB_2O_3$$

The energetic output of the combustion reaction could be printed as:

$$\Delta_cG(Al_nB_m) = -[½nG\,(Al_2O_3) + ½mG\,(B_2O_3) - G\,(Al_nB_m) - ¾\,(n + m)G\,(O_2)] = -\Delta_rG\,(Al_nB_m),$$

where G is Gibbs free energy of the corresponding compound.

The Gibbs free energies of combustion for Al_nB_m nanoclusters are presented as an interpolated two-dimensional heatmap (Fig. 3a). It shows the thermodynamic stability of the clusters. Here, $\Delta_c G(Al_nB_m)$ is taken with the opposite sign of the Gibbs free energy change, so that larger positive values correspond to more exothermic and thus more thermodynamically stable combustion. Figure 3b illustrates the specific combustion energy:

$$\Delta_c Q(Al_nB_m) = \Delta_c G(Al_nB_m)/M(Al_nB_m),$$

where $M(Al_nB_m)$ is the molar mass of the Al_nB_m cluster. This quantity characterizes how intensely a given cluster “burns” per unit mass and allows direct comparison between clusters of different compositions.

Pure boron clusters exhibit larger values of the Gibbs free energy of combustion ($\Delta_c G$) than aluminum clusters, which is in contrast to their bulk phases, in which aluminum combustion releases more energy: $\Delta_c G(Al_2O_3)$ = 1690.96 kJ/mol, $\Delta_c G(B_2O_3)$ = 1288.12 kJ/mol. This reverse behaviour at the nanoscale occurs due to dangling B-B bonds, making the surface energy of boron clusters very high.

Owing to the lower atomic mass of boron B-rich Al_nB_m nanoclusters exhibit the highest specific combustion energy, $\Delta_c Q$ (Fig. 3b). In addition, smaller clusters display enhanced values of $\Delta_c Q$, reflecting the increased fraction of under-coordinated surface atoms.

4. Conclusions

In this work, we performed a systematic investigation of Al-B nanoclusters containing up to 16 atoms. Despite the isoelectronic nature of aluminum and boron, it is shown that their structural chemistry differs significantly both from each other and from that of mixed Al-B clusters. Pure aluminum clusters are prone to easy disruption of metallic bonding and the formation of weak delocalized interactions, whereas boron clusters tend to form multicenter covalent bonds. The structural motifs of Al-B clusters are determined by the interplay between directional B-B bonding and metallic interactions involving Al atoms. As a result, a structural evolution is observed from aluminum-rich frameworks to dense boron networks.

Stability analysis shows that mixed Al-B clusters are locally stable, while fragmentation predominantly occurs through the loss of aluminum atoms, indicating stronger bonding within boron-rich frameworks. The highest stability is found for families of clusters satisfying the relation $n + m = 2k$, k = 6, 12, 16, 18, 20, and 22, corresponding to closed electronic shells. However, additional stabilization is also observed for clusters with an odd number of electrons due to high structural symmetry, which leads to enhanced local stability.

The combustion energetics reveal a pronounced nanoscale effect: boron-rich clusters exhibit higher Gibbs free energies of combustion and higher specific combustion energies than aluminum clusters, in contrast to the behavior observed in the bulk. This effect is associated with the low atomic mass of boron as well as the increased contribution of surface energy to the energetic characteristics of boron-

containing clusters at the nanoscale. Accordingly, nanostructured covalently bonded materials, such as aluminum–boron clusters, may be of interest as high-energy additives to energetic mixtures due to the enhanced contribution of surface energy and their distinct structural chemistry compared to single-element clusters.

Declarations

Conflicts of interest

The authors declare no competing financial interest.

Author Contribution

E.E.V. conceived the study, performed the structure prediction and quantum-chemical calculations, analyzed the data, and wrote the original draft of the manuscript. A.A.M. contributed to the methodology, data analysis, and manuscript editing. S.V.L. contributed to the conceptualization, methodology, analysis and interpretation of the results. A.P.M. contributed to the interpretation of the results and manuscript editing. A.R.O. supervised the project, contributed to the conceptualization and interpretation of the results, and critically revised the manuscript. All authors reviewed and approved the final manuscript.

Acknowledgement

This work was supported by the Russian Science Foundation (grant #25-43-20043). The calculations were performed on Oleg and Arkuda supercomputers at Skoltech and at the Joint Supercomputer Center of Russian Academy of Sciences and the Lobachevsky cluster at the University of Nizhny Novgorod.

References

1. I.A.S. Ferrão, M.A.A. Mendes, A.S.O.H. Moita, A.R.R. Silva, The addition of particles to an alternative jet fuel, Fuels 3 (2022) 184–206. https://doi.org/10.3390/fuels3020012.
2. M. Jones, C.H. Li, A. Afjeh, G. Peterson, Experimental study of combustion characteristics of nanoscale metal and metal oxide additives in biofuel (ethanol), Nanoscale Res Lett 6 (2011) 246. https://doi.org/10.1186/1556-276X-6-246.
3. D. Sundaram, V. Yang, R.A. Yetter, Metal-based nanoenergetic materials: Synthesis, properties, and applications, Prog. Energy Combust. Sci. 61 (2017) 293–365. https://doi.org/10.1016/j.pecs.2017.02.002.
4. A. Ulas, K.K. Kuo, C. Gotzmer, Ignition and combustion of boron particles in fluorine-containing environments, Combust. Flame 127 (2001) 1935–1957. https://doi.org/10.1016/s0010-2180(01)00299-1.

5. Q. Hu, Z. Wang, Z. Sun, Aluminum-based alloy fuels for solid propellants: Intrinsic properties, energy enhancement and combustion rate regulation, J. Alloys Compd. 1010 (2025) 177793. https://doi.org/10.1016/j.jallcom.2024.177793.
6. W. Pang, L.T. De Luca, X. Fan, O.G. Glotov, F. Zhao, Boron-based fuel-rich propellant: Properties, combustion, and technology aspects, CRC Press, 2019. https://doi.org/10.1201/9780429030680.
7. (n.d.). https://doi.org/10.1134/S199079311501008X.
8. B.I. Lukhovitskii, A.S. Sharipov, Thermodynamic analysis of prospects for using aluminum- and boron-containing clusters in combined high-energy fuels, J. Eng. Phys. Thermophys. 91 (2018) 766–773. https://doi.org/10.1007/s10891-018-1799-7.
9. X.-J. Feng, Y.-H. Luo, Structure and stability of Al-doped boron clusters by the density-functional theory, J Phys Chem A 111 (2007) 2420–2425. https://doi.org/10.1021/jp0656429.
10. S. Jin, B. Chen, X. Kuang, C. Lu, W. Sun, X. Xia, G.L. Gutsev, Structural and electronic properties of medium-sized aluminum-doped boron clusters $AlB_n$and their anions, J. Phys. Chem. C Nanomater. Interfaces 123 (2019) 6276–6283. https://doi.org/10.1021/acs.jpcc.9b00291.
11. G. Kresse, J. Furthmüller, Efficient iterative schemes for ab initio total-energy calculations using a plane-wave basis set, Phys. Rev. B Condens. Matter 54 (1996) 11169–11186. https://doi.org/10.1103/physrevb.54.11169.
12. G. Kresse, J. Hafner, Ab initio molecular dynamics for liquid metals, Phys. Rev. B Condens. Matter 47 (1993) 558–561. https://doi.org/10.1103/physrevb.47.558.
13. P.E. Blöchl, Projector augmented-wave method, Phys. Rev. B Condens. Matter 50 (1994) 17953–17979. https://doi.org/10.1103/physrevb.50.17953.
14. J.P. Perdew, K. Burke, M. Ernzerhof, Generalized gradient approximation made simple, Phys. Rev. Lett. 77 (1996) 3865–3868. https://doi.org/10.1103/PhysRevLett.77.3865.
15. M.J. Frisch, G.W. Trucks, H.B. Schlegel, G.E. Scuseria, M.A. Robb, J.R. Cheeseman, G. Scalmani, V. Barone, G.A. Petersson, H. Nakatsuji, Gaussian 16, Revision C.01, Gaussian, Inc., Wallingford CT, 2016.
16. A.D. Becke, Density-functional thermochemistry. III. The role of exact exchange, J. Chem. Phys. 98 (1993) 5648–5652. https://doi.org/10.1063/1.464913.
17. C. Lee, W. Yang, R.G. Parr, Development of the Colle-Salvetti correlation-energy formula into a functional of the electron density, Phys. Rev. B Condens. Matter 37 (1988) 785–789. https://doi.org/10.1103/PhysRevB.37.785.
18. P.J. Stephens, F.J. Devlin, C.F. Chabalowski, M.J. Frisch, Ab initio calculation of vibrational absorption and circular dichroism spectra using density functional force fields, J. Phys. Chem. 98 (1994) 11623–11627. https://doi.org/10.1021/j100096a001.
19. D.V. Rybkovskiy, S.V. Lepeshkin, A.A. Mikhailova, V.S. Baturin, A.R. Oganov, Lithiation of phosphorus at the nanoscale: a computational study of LiP clusters, Nanoscale 16 (2024) 1197–1205. https://doi.org/10.1039/d3nr05166h.

20. E.E. Vaneeva, S.V. Lepeshkin, A.R. Oganov, Prediction and Rationalization of Abundant C-N-H Molecules in Different Environments, J. Phys. Chem. Lett. 14 (2023) 8367–8375. https://doi.org/10.1021/acs.jpclett.3c01753.
21. A.A. Mikhailova, S.V. Lepeshkin, V.S. Baturin, A.P. Maltsev, Y.A. Uspenskii, A.R. Oganov, Ultralow reaction barriers for CO oxidation in Cu-Au nanoclusters, Nanoscale 15 (2023) 13699–13707. https://doi.org/10.1039/d3nr02044d.
22. M. Fedyaeva, S. Lepeshkin, A.R. Oganov, Stability of sulfur molecules and insights into sulfur allotropy, Phys. Chem. Chem. Phys. 25 (2023) 9294–9299. https://doi.org/10.1039/d2cp05498a.
23. D.V. Rybkovskiy, S.V. Lepeshkin, V.S. Baturin, A.A. Mikhailova, A.R. Oganov, Phosphorus nanoclusters and insight into the formation of phosphorus allotropes, Nanoscale 15 (2023) 1338–1346. https://doi.org/10.1039/d2nr06523a.
24. S.V. Lepeshkin, V.S. Baturin, Y.A. Uspenskii, A.R. Oganov, Method for Simultaneous Prediction of Atomic Structure and Stability of Nanoclusters in a Wide Area of Compositions, J. Phys. Chem. Lett. 10 (2019) 102–106. https://doi.org/10.1021/acs.jpclett.8b03510.
25. S.V. Lepeshkin, V.S. Baturin, A.S. Naumova, A.R. Oganov, “Magic” Molecules and a New Look at Chemical Diversity of Hydrocarbons, J. Phys. Chem. Lett. 13 (2022) 7600–7606. https://doi.org/10.1021/acs.jpclett.2c02098.
26. E.E. Vaneeva, S.V. Lepeshkin, D.V. Rybkovskiy, A.R. Oganov, Exploring the diversity of molecular carbon oxides, and their potential as high energy density materials, Mater. Today Energy 49 (2025) 101821. https://doi.org/10.1016/j.mtener.2025.101821.
27. B.I. Loukhovitski, A.S. Sharipov, A.M. Starik, Quantum chemical study of small Al n B m clusters: Structure and physical properties, Chem. Phys. 493 (2017) 61–76. https://doi.org/10.1016/j.chemphys.2017.06.006.
28. E.D. Anisimova, E.E. Vaneeva, V.S. Baturin, S.V. Lepeshkin, A.R. Oganov, Structural motifs and evolution of boron nanoclusters, J. Cluster Sci. 36 (2025). https://doi.org/10.1007/s10876-025-02815-0.
29. A.J. Mannix, X.-F. Zhou, B. Kiraly, J.D. Wood, D. Alducin, B.D. Myers, X. Liu, B.L. Fisher, U. Santiago, J.R. Guest, M.J. Yacaman, A. Ponce, A.R. Oganov, M.C. Hersam, N.P. Guisinger, Synthesis of borophenes: Anisotropic, two-dimensional boron polymorphs, Science 350 (2015) 1513–1516. https://doi.org/10.1126/science.aad1080.
30. H. Wu, H. Zhang, L. Geng, Y. Jia, B. Huang, M. Yang, B. Yin, X. Lei, Z. Luo, Pure metal clusters with atomic precision for nanomanufacturing, Nanomanufacturing Metrol. 5 (2022) 230–239. https://doi.org/10.1007/s41871-022-00139-5.

Figures

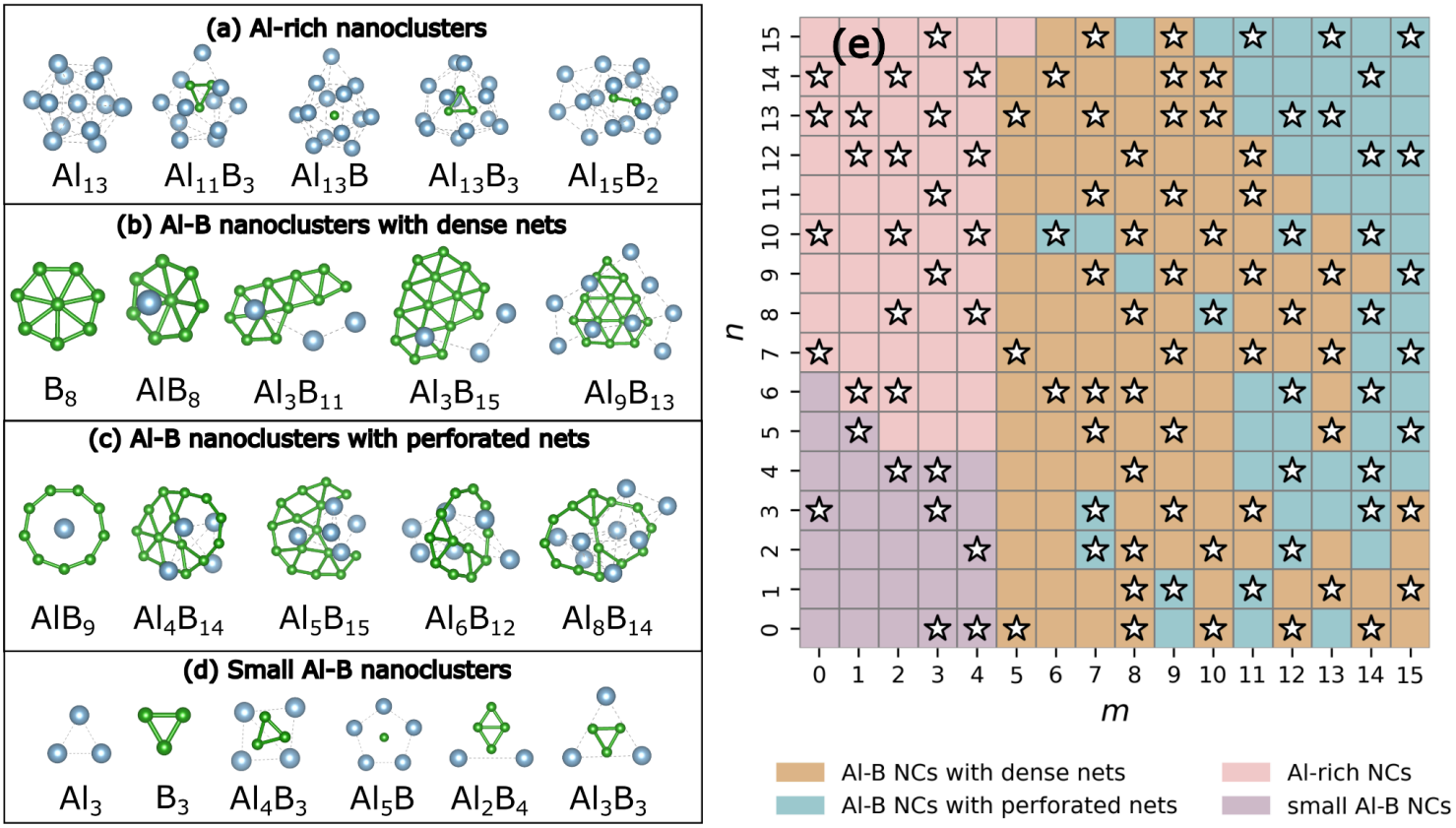


Figure 1

Classification of Al_nB_m clusters into four categories based on their structural topology, illustrated using representative examples with $\Delta^2_{min} > 0$: (a) Al-rich nanoclusters, (b) nanoclusters with dense networks, (c) nanoclusters with perforated networks, and (d) small Al–B nanoclusters. Blue and green spheres represent aluminum and boron atoms, respectively. (e) Schematic classification of Al_nB_m nanoclusters, where the composition space is divided into four regions according to structural characteristics. Stars indicate “magic” stoichiometries.

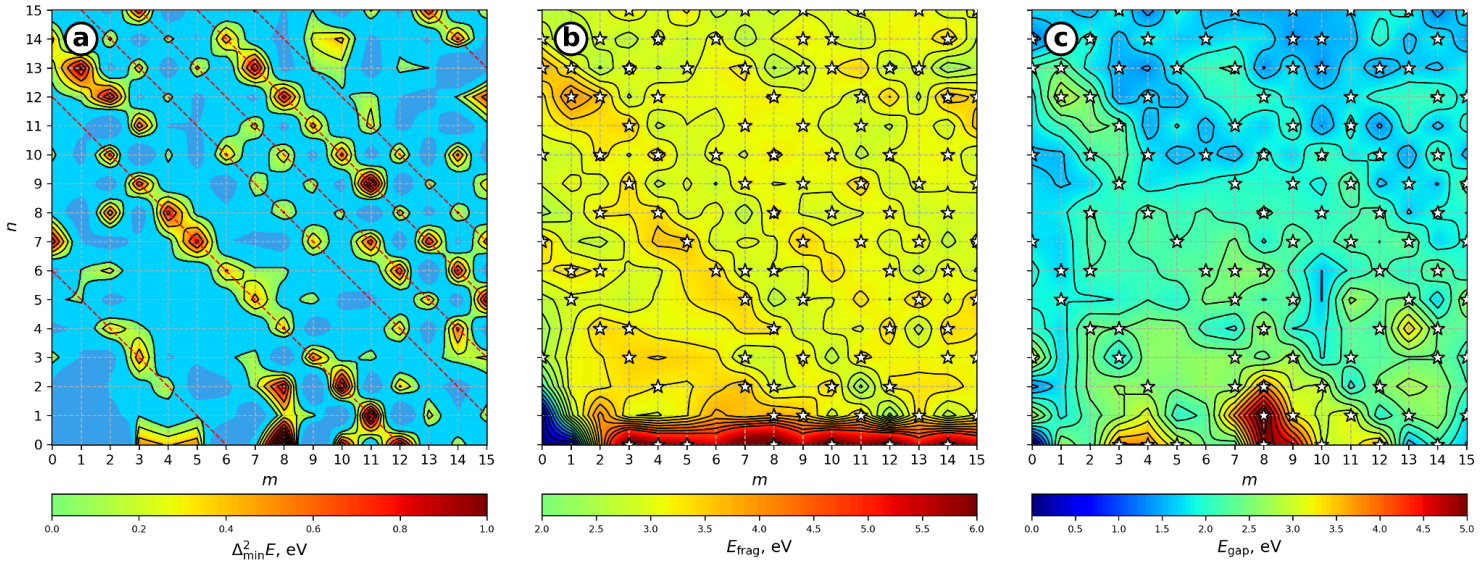


Figure 2

Interpolated heatmaps of (a) Δ^2_{min} and (b) E_{frag} (c) HOMO-LUMO gap (in eV) for Al_nB_m nanoclusters as functions of n and m. Regions of structural instability are highlighted in blue. The dashed reference lines indicate “magic” nanoclusters located along the diagonals $n + m$ = 6, 12, 16, 18, 20, and 22.

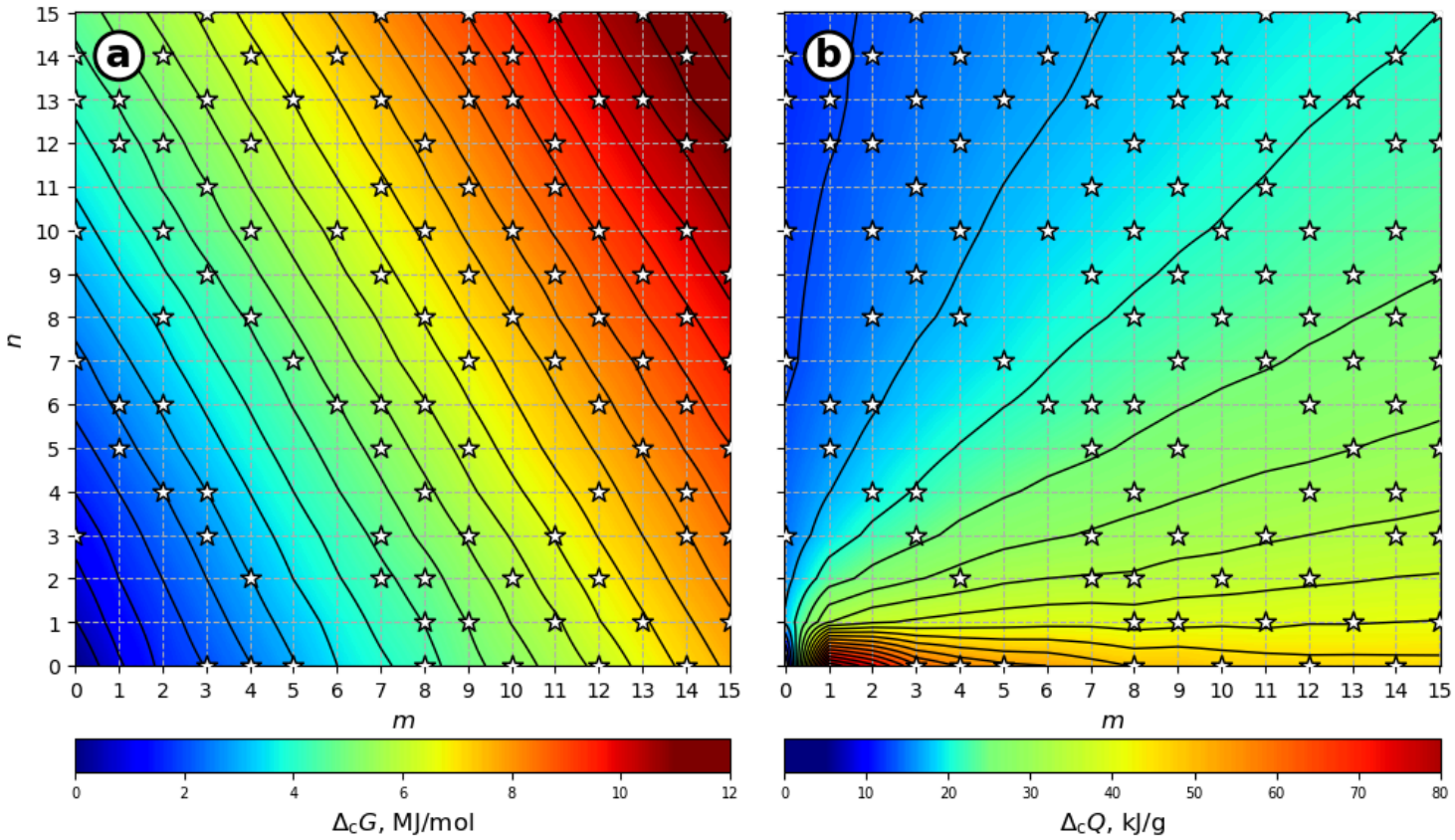


Figure 3

Interpolated heatmaps of (a) Gibbs free energies of combustion, Δ_cG and (b) specific combustion energy, Δ_cQ for A_nB_m nanoclusters. Stars highlight "magic" compositions of corresponding systems.

Supplementary Files

This is a list of supplementary files associated with this preprint. Click to download.

- AlBESIfinal.pdf